
ON CRACK PROPAGATION AND FAILURE MODES IN FIBER-REINFORCED CONCRETE SLABS

R. Felicetti, P.G. Gambarova and N. Zanini
Department of Structural Engineering, Milan University of Technology
Milan, Italy

Abstract

Concrete slabs subject to punching exhibit most of the characteristic problems ensuing from concrete brittleness and non-local nature, such as crack localization, snap-back tendency (in shear-sensitive slabs), and different failure modes.

In order to assess to what extent crack propagation and failure modes are altered by the introduction of a reinforcement (either fibers or a steel net), 82 relatively-thick slab specimens made of plain, fiber-reinforced and net-reinforced concrete were tested recently in Milan, under static and dynamic punching. Here reference is made mostly to the static tests, whose results are in the form of (a) load-displacement curves for different fiber or steel contents; (b) deflection profiles at various load levels; (c) crack patterns due to bending and shear. The results bring in new evidence on structural ductility, crack evolution and dynamic effects in slab punching.

1 Introduction and nature of problem

Concrete slabs have lately been the subject of several studies and papers regarding a variety of topics, such as: load-displacement response for various geometries and restraint conditions; strength and post-peak behavior; crack formation, propagation and localization (see the closely

related paper by Li and Bazant, 1993); resistant mechanisms; failure modes and size effect (Bazant and Cao, 1987); strain-rate sensitivity (Miyamoto et al., 1991); fiber and reinforcement effects (Absi, 1994; Chen et al., 1990, Walraven et al., 1992); static and dynamic punching (Mindess and Yan, 1993; Toutlemonde, 1993). In spite of such efforts, several aspects of slab behavior are still open to investigation, particularly in the domain of shear-sensitive slabs, where - for instance - crack patterns and failure modes are quite different depending on parameters such as fiber content and impact velocity (Gambarova and Schumm, 1994).

Here the attention is focused on (a) the resistant mechanisms in circular slabs subject to static punching; (b) the structural ductility, which depends on fiber or reinforcement content; (c) the collapse modalities, which bring in different crack patterns (radial cracking and cone-shaped cracking); (d) the evolution of cracking in displacement-controlled loading processes; and (e) the different energy-absorption capabilities of FRC slabs subject to static and dynamic punching.

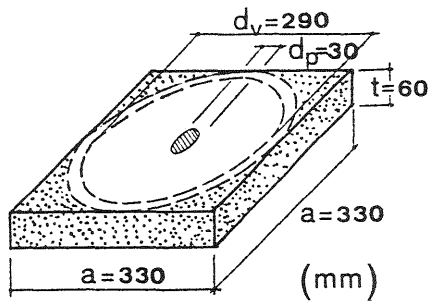
It was observed in previous tests on slab specimens subject to impact punching (Fig. 1, Gambarova and Schumm, 1994) that the collapse modalities of shear-sensitive slabs depend on the fiber content (PolyAcryloNitrile-PAN fibers), because of the higher strain-rate sensitivity of fiber-reinforced concretes, even for small fiber contents: as an example, a fiber content by volume of 1.5% can turn a bending-type collapse (Figs. 2a, b and 3a) into a punching-shear collapse (Figs. 2c and 3d). Similar results had been obtained by Miyamoto et al. (1991) with reference to impact velocity (higher impact velocities in plain concrete are equivalent to higher fiber contents, since fibers enhance concrete strain-rate sensitivity).

Since the impact tests did not allow the investigation of crack evolution during the loading process, a series of 34 static tests was planned and carried out, with different amounts and types of reinforcement, such as polyacrylonitrile and steel fibers, and steel nets.

2 Test philosophy

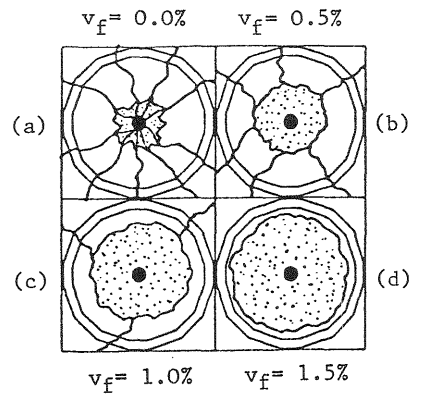
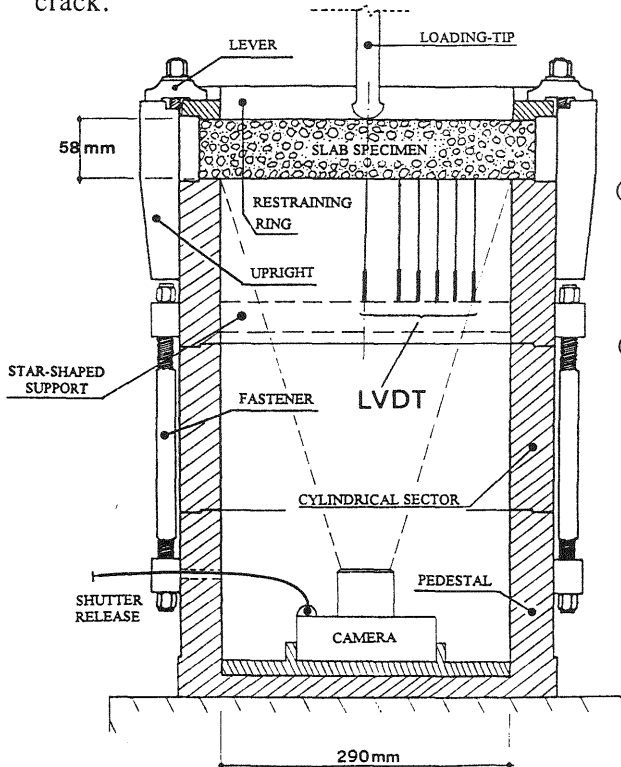
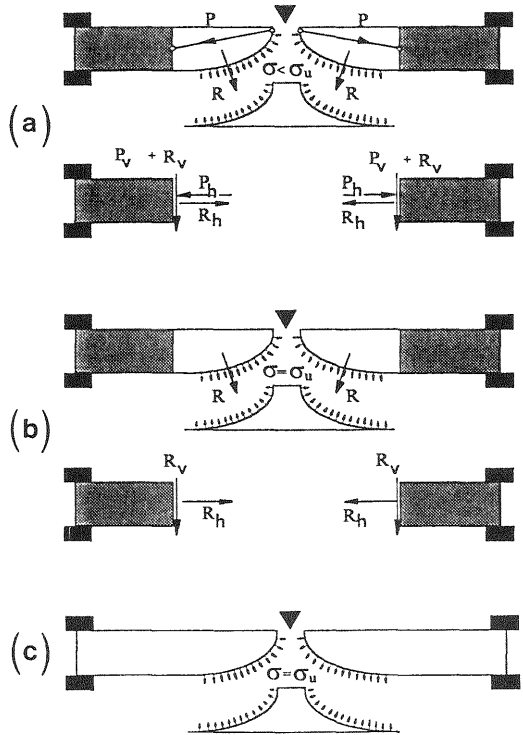
The choice of specimen dimensions is not as easy as it might appear, since several fundamental limitations come from the geometry and the capacity of the loading machine, from the maximum aggregate size (which should not be less than 12-15 mm in a concrete), from the length of the fibers or from the (minimum) diameter of the bars (not less than 5-6 mm in structural steel). Furthermore, in order to induce shear-sensitive behavior and to limit snap-back phenomena (caused by the unstable propagation of through cracks in the post-peak phase), the typical dimension (the net diameter in a circular slab) should not be more than 4-5 times the thickness, disregarding the dimension of the punching tip.

With d_a (max. aggregate size) = 15 mm, d_p (diameter of the punching tip) = $2d_a$ = 30 mm, P_u (press capacity) = 100 kN, suitable values for the



▲ Fig. 1 - Geometry of test specimens (static and dynamic tests): d_v = net diameter; d_p = loading-tip diameter. f_{cc} = 40 MPa (plain concrete).

► Fig. 2 - Possible resistant schemes at the onset of collapse: bending mechanism with in-plane (a) compressive forces, and (b) tensile forces + cohesive crack; (c) cohesive crack.



▲ Fig. 3 - Typical crack patterns at the bottom surface of slab specimens subjected to impact punching.

◀ Fig. 4 - Loading set-up.

thickness and net diameter are (Fig. 1):

$$t = (3-4)d_a = 45-60 \text{ mm}; d_v = d_p + (4-5)t = 210-330 \text{ mm}.$$

The nominal values $t = 60$ mm (reduced to 58 after polishing the upper surface of the specimen) and $d_v = 290$ mm were adopted ($d_v/t = 5$). Similar values for the ratio d_v/t appear in previous tests by Bazant and Cao (1987), $d_v/t = 5$, and by Greszczuk (1982), Jalil et al. (1994), Regan (1984), $d_v/t = 3-7$ (see Refs. in Zanini, 1994).

The 82 specimens tested so far have a square plan (side 330 mm, Fig. 1) and are clamped to a cylindrical support by means of a restraining ring (Fig. 4), in order to reproduce an axialsymmetric situation.

Among the 34 specimens subjected to static punching, 18 were reinforced with PAN fibers ($v_f=0.5, 1.0, 1.5\%$, $l_f=12, 24, 36$ mm, $d_f=30,100 \mu\text{m}$) and were tested mainly to make a comparison with previous impact tests.

The remaining 16 specimens were reinforced partly with PAN fibers ($v_f = 1.0, 1.5\%$, $l_f = 12$ mm, $d_f = 100 \mu\text{m}$), partly with DRAMIX fibers ($v_f = 1.0, 1.5\%$, $l_f = 30$ mm, $d_f = 500 \mu\text{m}$) and partly with a steel net ($p_x = p_y = 0.5, 1.0\%$, $\phi = 5, 6$ mm). In each sub-case, 2 nominally equal specimens were tested, together with 4 non-reinforced specimens.

3 Test set-up and instrumentation

All specimens (34) were clamped to a cylindrical body (Fig. 4), which was attached to the movable head (lower head) of a 8562 Instron press, fitted with an electromechanical actuator (capacity 100 kN). The punching tip was secured to the fixed head (= transverse beam). All tests were displacement-controlled (1 $\mu\text{m/s}$ up to the steeper part of the softening branch of the load-displacement curve, and 4 $\mu\text{m/s}$ afterward). The punching tip was fitted with 3 LVD transducers (2 appear in Fig. 5) in order to measure the penetration of the tip into the specimen (Fig. 5b) and the opening of the punching-shear crack (Fig. 5c).

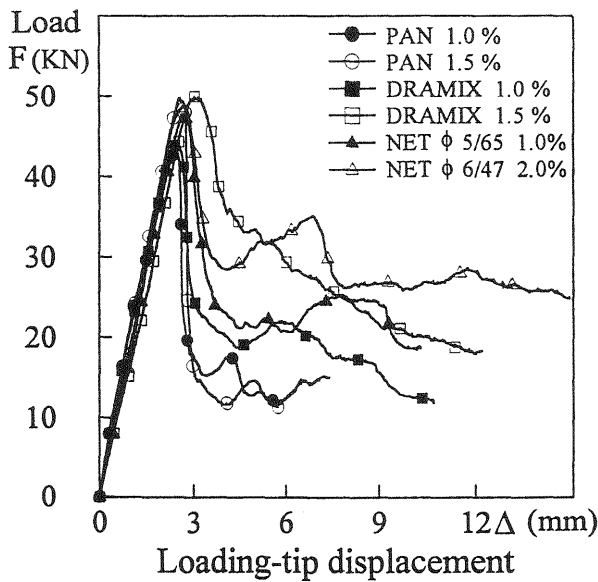
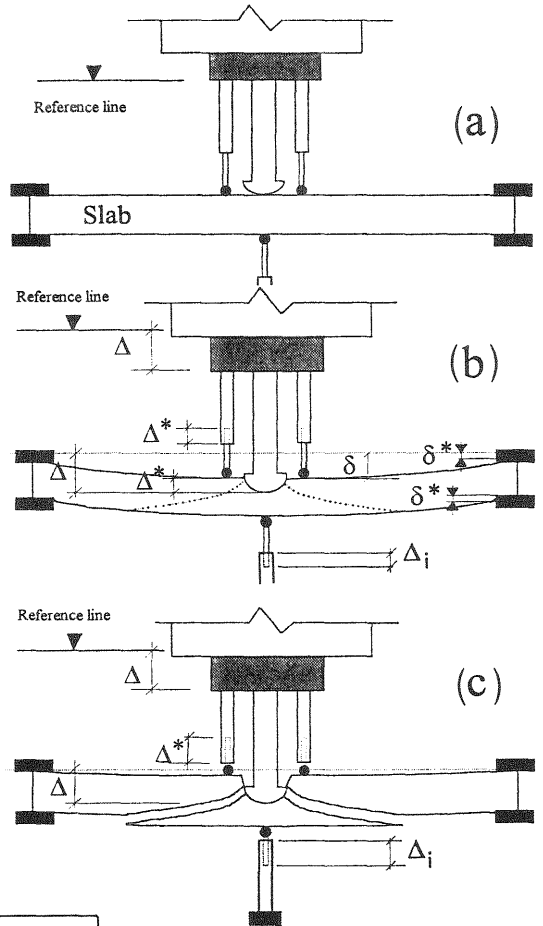
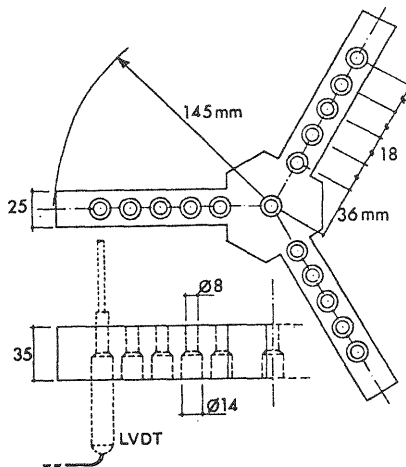
In 27 tests the displacements at the intrados (bottom surface) were measured by means of 16 LVD transducers held in position by a special star-shaped support (Fig. 6), which was fastened to the inner wall of the cylindrical body. In this way the displacement w was measured along three radial directions, at each step of the displacement-controlled loading process, and the three deflection curves, as well as the mean deflection curve (see Fig. 8) were reproduced on the screen of a P.C., thus making the control of the test more effective.

In 7 tests the star-shaped support and its transducers were removed, to make room for a camera (Fig. 4). As a result, the photographs of the crack pattern at the intrados and the singularities of the load-displacement curve could be brought into mutual relation.

The displacements were continuously monitored and registered by means of a data-acquisition unit (UPM 60), which was controlled by a P.C.

► Fig. 5 - Sketch of the loading-tip instrumentation and symbols adopted for the displacements:

- Δ = loading-tip displacement
- Δ^* = loading-tip penetration
- Δ_i = displacement at the intrados
- δ^* = settlement along the support (= 0)
- δ = displacement at the extrados (= $\Delta - \Delta^*$)



◀ ▲ Fig. 6 - Star-shaped support carrying 16 LVD transducers for measuring the displacements at the intrados of slab specimens.

◀ Fig. 7 - Load-displacement curves for different contents of polyacrylonitrile and steel fibers ($p = 1.0, 1.5\%$ by volume) and different reinforcement ratios (steel net with $p_x = p_y = 0.5, 1.0\%$).

4 Test results

Role of reinforcement content and type - Since the aspect ratio of the polymeric fibers (PAN fibers) has only limited influence on slab response (Zanini, 1994: $\lambda = 120-900$), the attention is focused here on the content and type of reinforcement (Fig. 7). As might have been expected, both the initial almost linear branch and the peak load were negligibly affected by the reinforcement, while the post-peak behavior was definitely softer at high reinforcement contents, as shown by the 2% steel net, compared to 1.5% of either PAN or DRAMIX fibers. High reinforcement contents limit the drop of the load-displacement curve after the peak, and make the softening branch more regular and predictable.

Failure modes - As a rule, the peak load was accompanied by the formation of a few radial cracks at the intrados, and the collapse was characterized by the detachment of a truncated cone (owing to punching-shear cracking). As shown by the deflection profiles (Fig. 8) at various load levels, the behavior tends to be linearly elastic up to 75% of the peak load, and the deflection tends to flatten-off in the central part of the slab, beyond 75% of the peak load (descending branch), as required by the formation of the punching-shear cone, which tends to behave like a rigid body. As a rule, the higher the reinforcement content, the milder is the transition from radial cracking to punching-shear cracking (Figs. 8a,b).

Punching-shear failures are characterized by the snap-back of the displacement at the extrados (Fig. 9a, full line) and by a residual inelastic displacement at the intrados (Fig. 9b, full line). On the contrary, bending-type failures exhibit no snap-back (Fig. 9a, dashed line) and the displacements at the extrados and at the intrados are fairly proportional to each other (Fig. 9b, dashed line).

Crack evolution - Radial cracking (with few and thin cracks, Fig. 10b) forms before the load peak, propagates at and beyond the load peak (Fig. 10a, full square at the left), but then the radial cracks tend to close, and a circumferential crack appears (Fig. 10c,d). The formation of the truncated cone is not blunt, but requires the dissipation of a considerable amount of energy (Fig. 10a, full square at the right). Such behavior was common to practically all static tests, and the residual strength during the formation of the cone was - broadly speaking - close to 60-66% of peak strength for the steel net, 40-45% for DRAMIX fibers and 20-25% for PAN fibers, compared to less than 20% for plain concrete.

Static-versus-dynamic behavior - Fig. 11 clearly shows the much larger energy dissipated during a dynamic test compared to a static test (PAN fibers). In the dynamic tests, the load was not cleared of the inertia force, but, since inertia effects were expected to be very limited because of slab thickness, the curves are indicative of the remarkable concrete strain-rate sensitivity (with or without fibers).

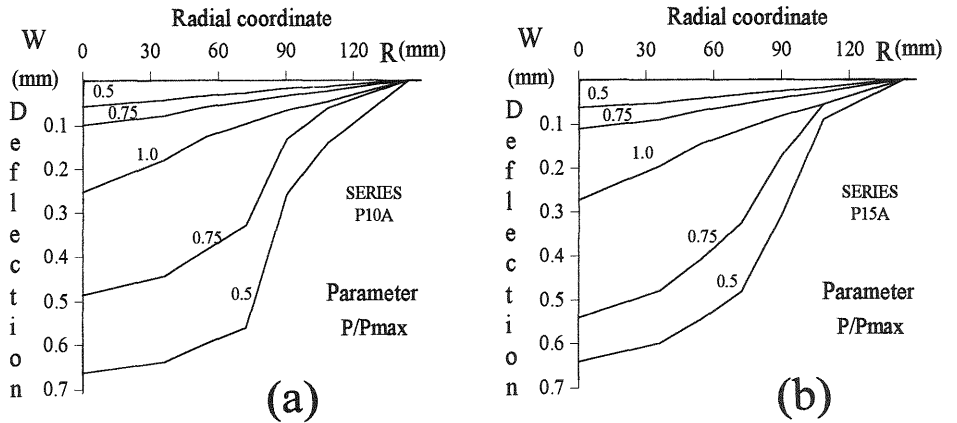


Fig. 8 - Diagrams of the deflection at various load levels. PAN fibers: fiber content by volume $v_f = 1.0, 1.5\%$; fiber length $l_f = 12$ mm; fiber diameter $d_f = 100$ μm .

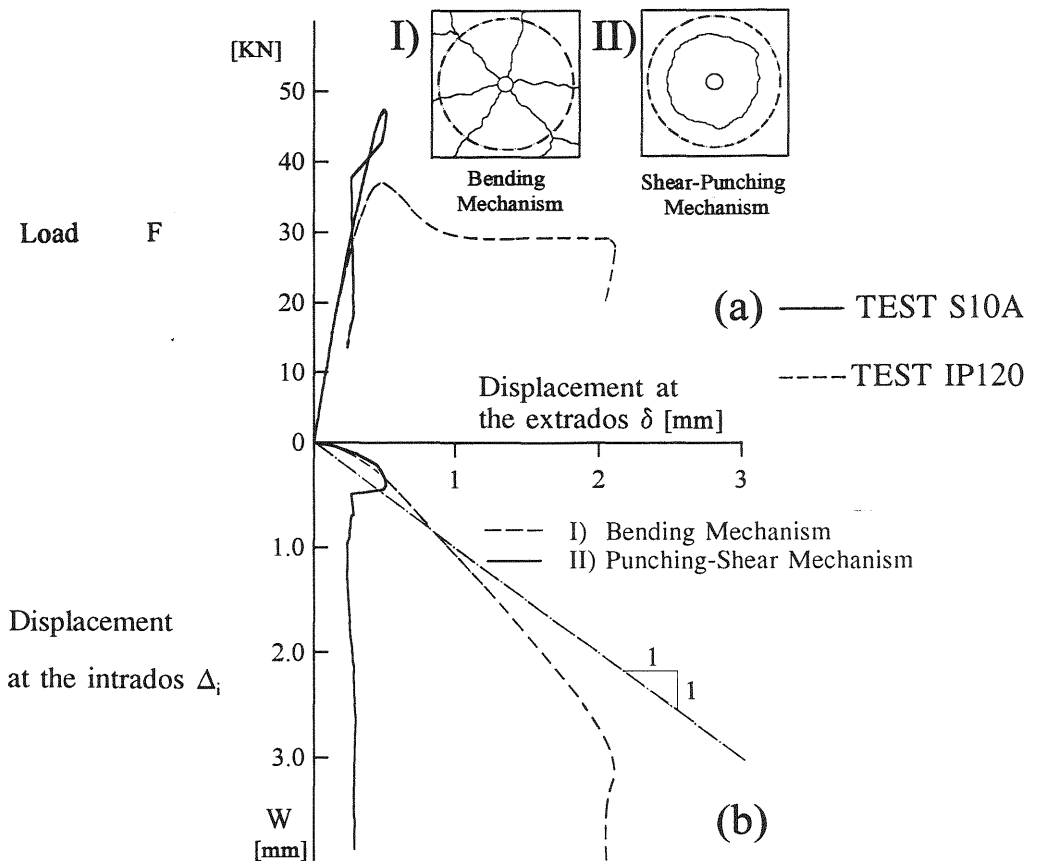


Fig. 9 - Typical load-displacement and displacement-displacement curves for punching failures characterized mostly by bending (I) and by shear (II): (a) load versus displacement at the extrados δ , and (b) displacement at the intrados Δ_i versus displacement at the extrados. PAN fibers, $v_f = 1\%$, $\lambda = 600$ in test S10A, $\lambda = 120$ in test IP120.

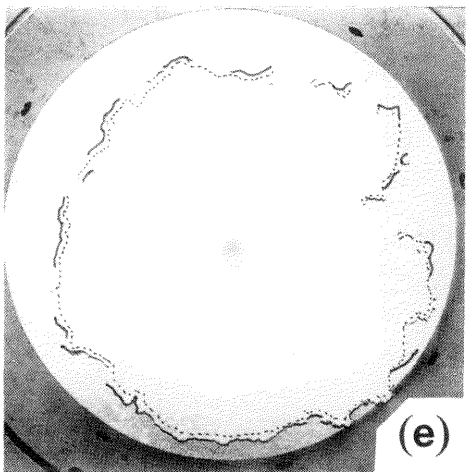
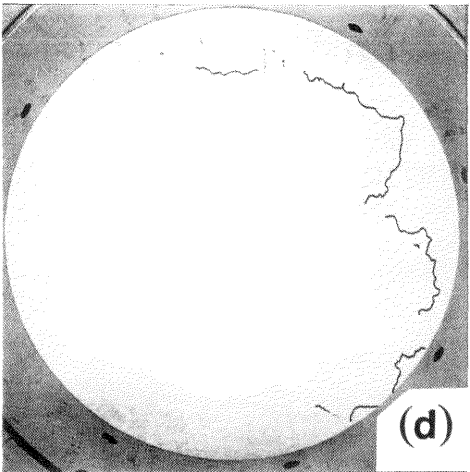
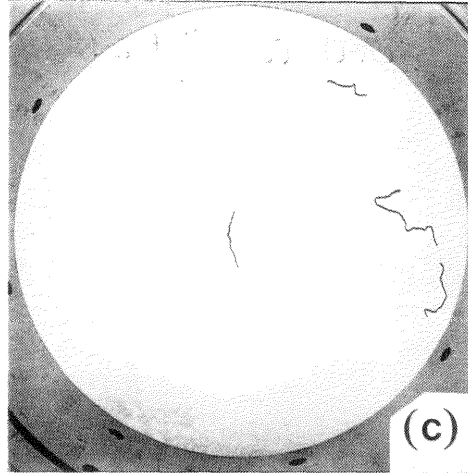
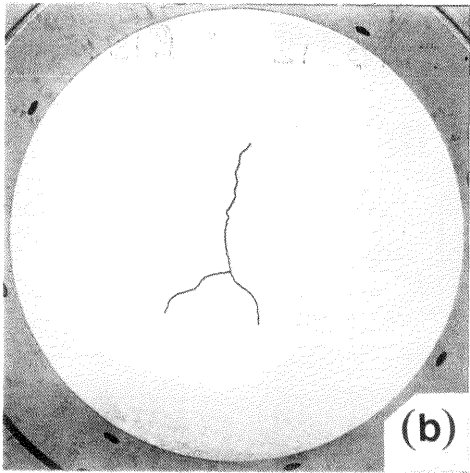
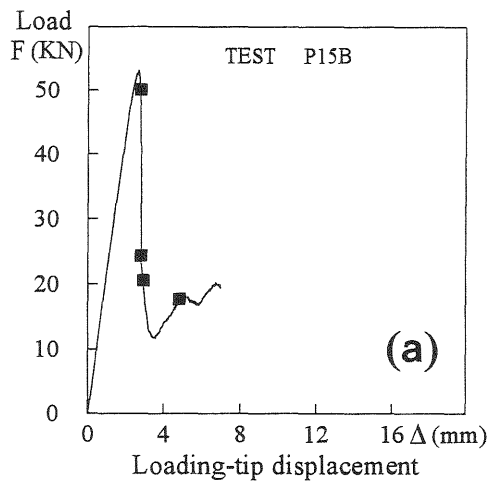


Fig. 10 - Typical evolution of crack pattern in static tests: (a) load-displacement curve of Test P15B (PAN fibers, fiber content 1.5% by volume, $l_f = 12$ mm, $d_f = 100 \mu\text{m}$); (b) bending cracks; (c) bending and shear cracks; (d, e) shear cracks. $P_{\max} = 53.1$ kN.

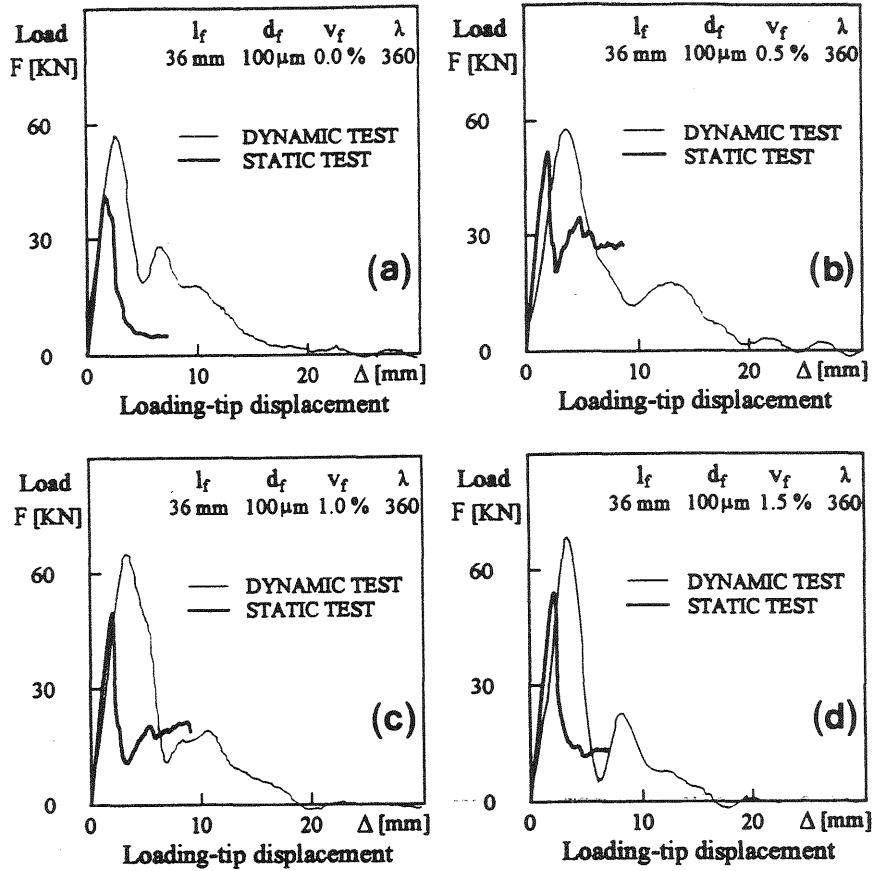


Fig. 11 - Load-displacement curves under static and dynamic punching (PAN fibers, impact velocity 2.65 m/s).

5 Concluding remarks

The results of this study can be summarized as follows:

1. Greater fiber contents lead to a higher structural ductility, both under static and dynamic loading; however, steel fibers and net reinforcement has more than a edge over PAN fibers;
2. In static tests the peak of the load-displacement response is always accompanied by the formation of more or less extended radial cracks, while the post-peak behavior is definitely characterized by the formation of a punching cone;
3. The type of failure (shear-bending failure with radial cracking, and punching-shear failure with cone-shaped cracking) can be identified during the test by comparing the displacements at the intrados and at the extrados of the slab;
4. Snap-back phenomena can be detected and measured even if the test is run by controlling the punching-tip displacement, since a kind of "mild" softening comes from the plastic deformation of the concrete, underneath the loading-tip.

Acknowledgements

The authors wish to acknowledge the financial support of the Italian National Council for Scientific Research - C.N.R. for this study, which was carried out within the Special Project "High-Performance Materials for Better Structures" (1994-95).

References

- Absi, E. (1994) Béton de fibres: synthèse des études et recherches réalisées au CEBTP. **Annales de l'Institut Technique du Batiment et des Travaux Publics**, Série Béton 305 (520), 85-127.
- Bazant, Z.P. and Cao, Z. (1987) Size effect in punching shear failure of slabs. **ACI Structural Journal**, 84 (1), 44-53.
- Chen, Y.J., Chen, H.L., Dancygier, A.N., Shah, S.P. and Keer, L.M. (1990) Tests of model reinforced-concrete circular slabs. **ACI Structural Journal**, 87 (6), 727-737.
- Gambarova, P.G. and Schumm, C.E. (1994) Impulsive punching of fiber-reinforced concrete slabs. **Proceedings of ASCE XIIth Structures Congress**, Atlanta (Ga, USA), 1, 252-257.
- Li, Y.N. and Bazant, Z.P. (1993) Penetration fracture of ice plate: 2-D analysis and size effect. **ASCE Journal of Engineering Mechanics**, 120 (7), 1481-1498.
- Mindess, S. and Yan, C. (1993) Perforation of plain and fibre reinforced concretes subjected to low-velocity impact loading. **Cement and Concrete Research**, 23, 83-92.
- Miyamoto, A., King, M.W. and Fujii, M. (1991) Analysis of failure modes for reinforced concrete slabs under impulsive loads. **ACI Structural Journal**, 88 (5), 538-545.
- Toutlemonde, F., Boulay, C. and Gourraud, C. (1993) Shock-tube tests of concrete slabs. **Materials and Structures**, 26, 38-42.
- Walraven, J.C., Pat, M.G.M. and Markov, I. (1992) The punching-shear resistance of fibre-reinforced concrete slabs. Report 22.5-92-6, Delft University of Technology, Stevin Laboratory.
- Zanini, N. (1994) On the static and impulsive punching of fiber-reinforced and net-reinforced concrete slabs, MS Thesis, Dept. of Structural Engineering, Milan University of Technology, October 1994.

Author Index

A

Adachi, H., 655
Adamson, R.M., 675
Ahn, T.S., 1155
Akesson, M., 899
Akita, H., 305, 1503
Akyüz, S., 1037
Ali, A., 1565
Alvaredo, A.M., 1423, 1469, 1529
Arslan, A., 45, 693

B

Bachmann, H., 1407
Baker, G., 929, 991
Barr, B.I.G., 3, 55
Bascoul, A., 571
Bazant, Z.P., 515, 841, 955, 1021, 1397
Benkhira, H., 343
Beranek, W.J., 965
Berra, M., 85
Bhattacharjee, S.S., 1057
Blaschke, F., 279
Blechman, I., 445
Bodé, L., 945, 1047
Bolander Jr., J.E., 375, 535
Bolzon, G., 885
Borst de, R., 871, 991, 1011
Boulay, C., 709
Brencich, A., 363
Brincker, R., 31
Brioschi, M.A., 1139
Brokenshire, D.R., 3

C

Cadoni, E., 1555
Canton, E., 1219
Carmeliet, J., 1011
Carmona, S., 769
Carol, I., 841
Carpinteri, A., 363, 557, 581, 1315
Casanova, P., 1169
Castellani, A., 85
Cervenka, J., 1285
Cervenka, V., 1387
Chang, T.P., 803
Cherednichenko, T., 1513
Chiaia, B., 581
Claeson, C., 1209
Cornelius Hansen, T., 1239
Courtade, R.M., 343

D

Delaplace, A., 981
Denarié, E., 239
Dempesey, J.P., 675
Dietermann, H.A., 729
Ding, J.-T., 119, 169, 597
Dortmans, L.J.M.G., 1261
Dubé, J.F., 1301

E

Elices, M., 75, 95, 1179
Eligehausen, R., 665, 1387, 1585
Elouard, A., 1169, 1443
Eo, S.H., 685

F

Felicetti, R., 813
Feltrin, G., 1407
Feng, N.-Q., 119, 169, 597
Ferrara, G., 1315
Ferro, G., 557
Foremsky, D.J., 1329
Fujiwara, T., 1503

G

Galli, M., 1407
Gallo, S., 1469
Gambarova, P.G., 813
Gao, J., 329
Garrecht, H., 719
Gerdes, A., 271
Gettu, R., 769
Ghavamian, S., 1301
Ghrib, F., 1057
Gils van, M.A.J., 1261
Goffi, L., 1189
Gopalaratnam, V.S., 769, 1155
Granger, L., 1493
Grimm, R., 125
Grummitt, C.A., 929
Guinea, G. V., 75, 95
Guo, Z.K., 179
Gyltoft, K., 1209

H

Hack, E., 229
Hakuno, M., 1369

Hasegawa, T., 857
Hawkins, N.M., 179, 685
Hilsdorf, H.K., 719
Hikosaka, H., 375
Hobbelman, G.J., 965
Horii, H., 1345
Hu, B., 505
Hu, X.-Z., 415
Huet, C., 239, 1089
Huerta, A., 945
Hwang, C.L., 803

I

Ikeda, K., 425
Ince, R., 693
Invernizzi, S., 557
Irobe, M., 495
Ishii, K., 645
Ishiguro, S., 145
Ito, T., 1125

J

Jamet, D., 769
Jefferson, A.D., 55
Jelinek, R., 729
Jirasek, M., 955, 1397
Ji, X.-H., 119, 597
Job, L., 239

K

Kabele, P., 1345
Kan, Y.-C., 111
Kang, H.-D., 397
Kanstad, T., 1459
Karihaloo, B.L., 1111
Kitsutaka, Y., 199
Klisinsky, M., 473
Kobashi, Y., 535
Kobayashi, A. S., 179
Koide, H., 305
König, G., 125
Kosai, M., 179
Kovler, K., 189
Koyanagi, W., 17, 1125
Kröplin, B., 825
Kurihara, N., 17, 1125
Kwak, G.-S., 685

L

La Broderie, Ch., 1047
Landis, E.N., 315
Larsson, R., 899

Lee, Y.-H., 397
Léger, P., 1057
Li, V.C., 1329
Liang, L., 1251
Libardi, W., 135
Lim, Y.M., 1329
Lin, C.-Y., 803
Lin, Y.M., 1251
Liu, Y.-Q., 375

M

Magureanu, C., 285
Maier, G., 885
Markeset, G., 435
Martinola, G., 1481
Maruyama, K., 425
Masuda, A., 745
Matsuo, S., 745
Matsuoka, S., 745
Mazars, J., 483, 1301
Mechtcherine, V., 719
Meftah, F., 1069
Mehlhorn, G., 279
Melchiorri, G., 1315
Menétrey, Ph., 1229
Merabet, O., 1069
Mier van, J.G.M., 45, 261, 295, 353, 383
Mihashi, H., 209, 755
Moriizumi, K., 645
Mulumule, S.V., 675

N

Nagano, R., 1079
Nakamura, H., 755
Nakanishi, M., 655
Nanakorn, P., 1345
Noghabai, K., 1575
Nomura, N., 209, 755
Noune, A., 343

O

Ogino, K., 655
Ohlsson, U., 473, 1545
Olofsson, T., 473, 1545
Ouyang, C., 135, 783
Ozbolt, J., 665, 1387

P

Pacios, A., 783
Pamin, J., 871
Peng, S.Y., 495
Pijaudier-Cabot, G., 945, 981, 1047

Planas, J., 75, 95, 1179
Plizzari, G.A., 1377
Polanco-Loria, M., 1027
Pontiroli, C., 1001, 1219
Prisco di, M., 483
Pukl, R., 1387, 1585

R

Reick, M., 1585
Reynouard, J.M., 1069
Rocco, C., 75
Roh, Y.-S., 251
Rokugo, K., 17, 1125
Rossi, P., 543, 709, 1169, 1199, 1271, 1443, 1493
Rouquand, A., 1001, 1219
Roux, S., 981
Ruiz, G., 1179
Runesson, K., 899

S

Sadouki, H., 229, 607, 619
Saouma, V.E., 251, 1285, 1377
Schlangen, E., 45, 353, 913
Schreyer, H.L., 329
Shah, S.P., 135, 315, 783
Shevchenko, V.I., 1513
Shieh, M.M., 803
Shirai, N., 495, 645, 655
Slowik, V., 251, 1529
Sluys, L.J., 729, 1139
Song, Y., 505
Sorensen, S.I., 1027
Stanzl-Tschegg, S.E., 145
Steiger, T., 229
Stroeven, P., 461
Sunderland, H., 239
Swartz, S.E., 111

T

Tailhan, J.L., 1047
Tang, T., 135
Tasdemir, C., 125
Tasdemir, M.A., 125, 1037
Tinawi, R., 1057
Tin-Loi, F., 885
Tolou, A., 239
Tomon, M., 305
Toutlemonde, F., 709, 1199
Travnicek, R., 145
Trunk, B., 607
Tschegg, E.K., 145
Turatsinze, A., 571

U

Uchida, Y., 17, 1125
Ulfkjær, J.P., 31
Ulm, F.-J., 543, 1271, 1443
Umeoka, T., 755

V

Valente, S., 1315
Vervuurt, A., 295, 353
Visser, J.H.M., 261
Vitek, P., 793
Vitek, J.L., 793
Vliet van, A., 353, 383

W

Wang, H., 415
Wang, M.L., 329
Weihe, S., 825
Willam, K., 397, 1079
With de, G., 1261
Wittmann, F.H., 271, 607, 619, 1469, 1481, 1519, 15
Wörmer, J.-D., 1539

X

Xi, Y., 635

Y

Yagust, Y.I., 1361
Yanagi, H., 745
Yang, S., 135
Yankelevsky, D.Z., 1361
Yoshikawa, H., 1079

Z

Zaitsev, Y., 1513
Zanini, N., 813
Zeitler, R., 1539
Zhao, G., 505
Zhou, F.P., 65, 219, 1315
Zhuang, Q.-F., 119, 169, 597

